Nanoscale Research Letters
a SpringerOpen Journal

NANO EXPRESS Open Access

Hydrothermal phase transformation of hematite to magnetite

Jie-feng Lu and Cho-Jen Tsai*

Abstract

Different phases of iron oxide were obtained by hydrothermal treatment of ferric solution at 200°C with the addition of either KOH, ethylenediamine (EDA), or KOH and EDA into the reaction system. As usually observed, the α-Fe_2O_3 hexagonal plates and hexagonal bipyramids were obtained for reaction with KOH and EDA, respectively. When both KOH and EDA were added into the reaction system, we observed an interesting phase transformation from α-Fe_2O_3 to Fe_3O_4 at low-temperature hydrothermal conditions. The phase transformation involves the formation of α-Fe_2O_3 hexagonal plates, the dissolution of the α-Fe_2O_3 hexagonal plates, the reduction of Fe^{3+} to Fe^{2+}, and the nucleation and growth of new Fe_3O_4 polyhedral particles.

Keywords: Iron oxides; Hydrothermal; Phase transformation

Background

The more stable phases in iron oxides are hematite and magnetite. Hematite can be used in a lot of applications, such as sensors [1], water photooxidation [2], drug delivery [3], lithium ion battery [4], pigmentation [5], solar cell [6], etc., and magnetite can be utilized in biomedicine [7-11], magnetic devices [12], etc. Therefore, studies about the nano/microstructures of iron oxides and their properties, which are related to the intrinsic structure and crystal shapes, have been intensively engaged, especially for hematite and magnetite. The bandgap of hematite is 2.0 to 2.2 eV which makes it useful in applications that involve visible light absorption [13,14]. Magnetite has unique electric and magnetic properties because its intrinsic crystal structure allows electrons to be transferred between Fe^{2+} and Fe^{3+} in the octahedral sites [15].

Many researches have demonstrated the capability of using chemical syntheses to control particle morphologies of iron oxide by surfactants [16-18]. Morphologies like wires [19], rods [20], tubes [21], rings [22], disks [23], cubes [24], spheres [25], hexagonal plates of α-Fe_2O_3 [26,27], and polyhedral particles of Fe_3O_4 [28,29] have been synthesized successfully.

Several robust methods have been developed for phase transformation of iron oxides. α-Fe_2O_3 can be transformed to Fe_3O_4 at high temperature under a reducing ambient, such as hydrogen ambient [30,31]. Yanagisawa and Yamasaki also showed that by controlling the mineralizer solutions, temperatures, and partial pressures of hydrogen in a hydrothermal system, phase transformation from α-Fe_2O_3 to Fe_3O_4 particles can be achieved [32]. The result indicated that high temperature and high pressure of hydrogen can accelerate the reduction reaction.

Phase transition of iron oxides can also take place by hydrothermal reaction with a reducing agent [33,34]. Sapieszko and Matijewic had observed a similar phase transformation from α-Fe_2O_3 hexagonal plates to octahedral Fe_3O_4 particles triggered by the addition of hydrazine which is used as an antioxidant [35] during hydrothermal process.

In this experiment, we explore the role of ethylenediamine (EDA or en in ligand form) on the phases of iron oxide in hydrothermal condition. EDA is usually considered to be the chelating agent or to function as a ligand to facilitate the growth of particles under hydrothermal reaction [36,37]. However, phase transformation of iron oxide was observed when EDA was added into the alkaline solution. Thus, a special low-temperature route for the transformation of α-Fe_2O_3 to Fe_3O_4 was provided. The phase and shape variations with the addition of

* Correspondence: cjtsai@mx.nthu.edu.tw
Department of Material Science and Engineering, National Tsing-Hua University, Hsinchu 30013, Taiwan

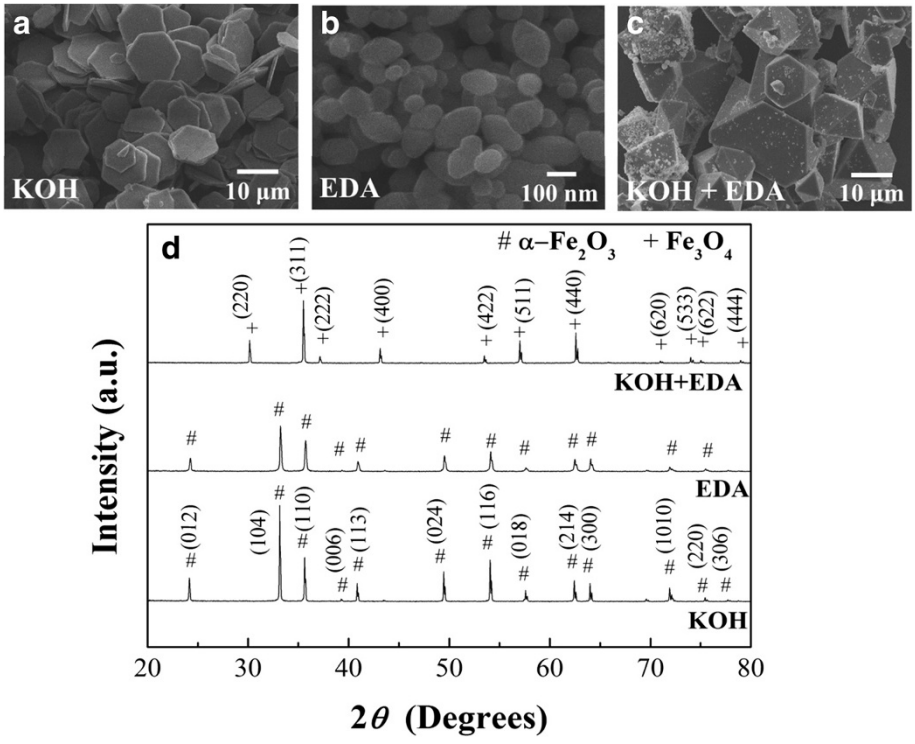

Figure 1 SEM images and corresponding XRD patterns of iron oxide particles. SEM images of iron oxide particles prepared with the addition of **(a)** 5 ml of 10.67 M KOH, **(b)** 1 ml of EDA, and **(c)** both 5 ml of 10.67 M KOH and 1 ml of EDA into the ferric solutions. **(d)** The corresponding XRD patterns of the iron oxide particles obtained for the cases of **(a)**, **(b)**, and **(c)**.

potassium hydroxide (KOH), EDA, and KOH and EDA were investigated and compared.

Methods

Ferric nitrate ($Fe(NO_3)_3 \cdot 9H_2O$), 1 mmol, was dissolved in 10 ml of distilled water to form a transparent yellow solution. Next, three different mineralizing agents were added into the ferric solution. First is 5 ml of 10.67 M KOH aqueous solution. The solution was added dropwisely into the ferric solution. Second is 1 ml of EDA. The EDA was added gradually into the ferric solution. Third is the combination of KOH and EDA. The 10.67 M KOH solution, 5 ml, was added first followed by the addition of 1 ml of EDA. After adding these mineralizing agents, a brown $Fe(OH)_3$ suspension was obtained. Then, these solutions were all stirred for 30 min before transferring the mixture into a Teflon-lined stainless steel autoclave (DuPont, Wilmington, DE, USA) of 40-ml capacity and followed by heat treatments at 200°C for 9 h. After that, the autoclave was cooled down to room temperature in air. The precipitates were collected by centrifugation, washed with deionized water and ethanol several times to remove organic and impurities, and finally dried in air at 80°C for 12 h.

The as-synthesized powder was characterized by X-ray diffraction (XRD) with Cu-Kα radiation, field emission scanning electron microscopy (FE-SEM), transmission electron microscopy (TEM), and Raman spectroscopy. The magnetic properties were measured by a vibrating sample magnetometer (VSM) with a maximum magnetic field of 1.5 kOe.

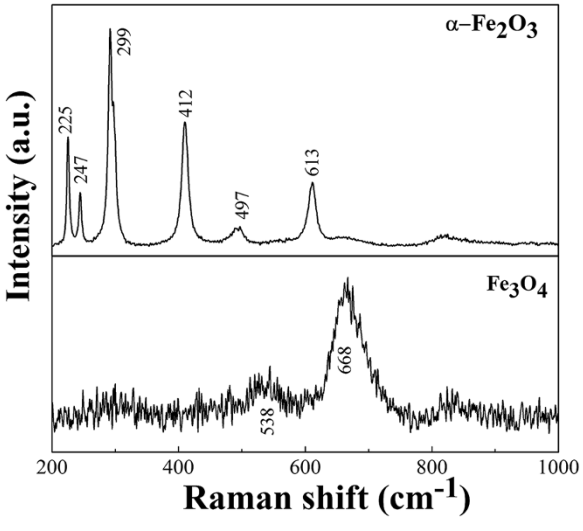

Figure 2 Raman spectra of α-Fe_2O_3 hexagonal plates and Fe_3O_4 polyhedral particles.

Results and discussion

Figure 1 shows the iron oxide particles synthesized with three different reducing agents, KOH, EDA, and KOH/EDA, under a hydrothermal condition of 200°C for 9 h in the ferric solution. Figure 1a shows the α-Fe_2O_3 hexagonal plates which were obtained with the addition of KOH, and Figure 1b shows the α-Fe_2O_3 hexagonal bipyramid particles obtained when EDA was added into the system. Figure 1c shows the Fe_3O_4 polyhedral particles obtained with the addition of both KOH and EDA into the reaction system. (When NaOH substitutes for KOH, a similar reaction would occur.) The crystal structure of these iron oxide particles was analyzed by XRD and is shown in Figure 1d. The phase can be identified

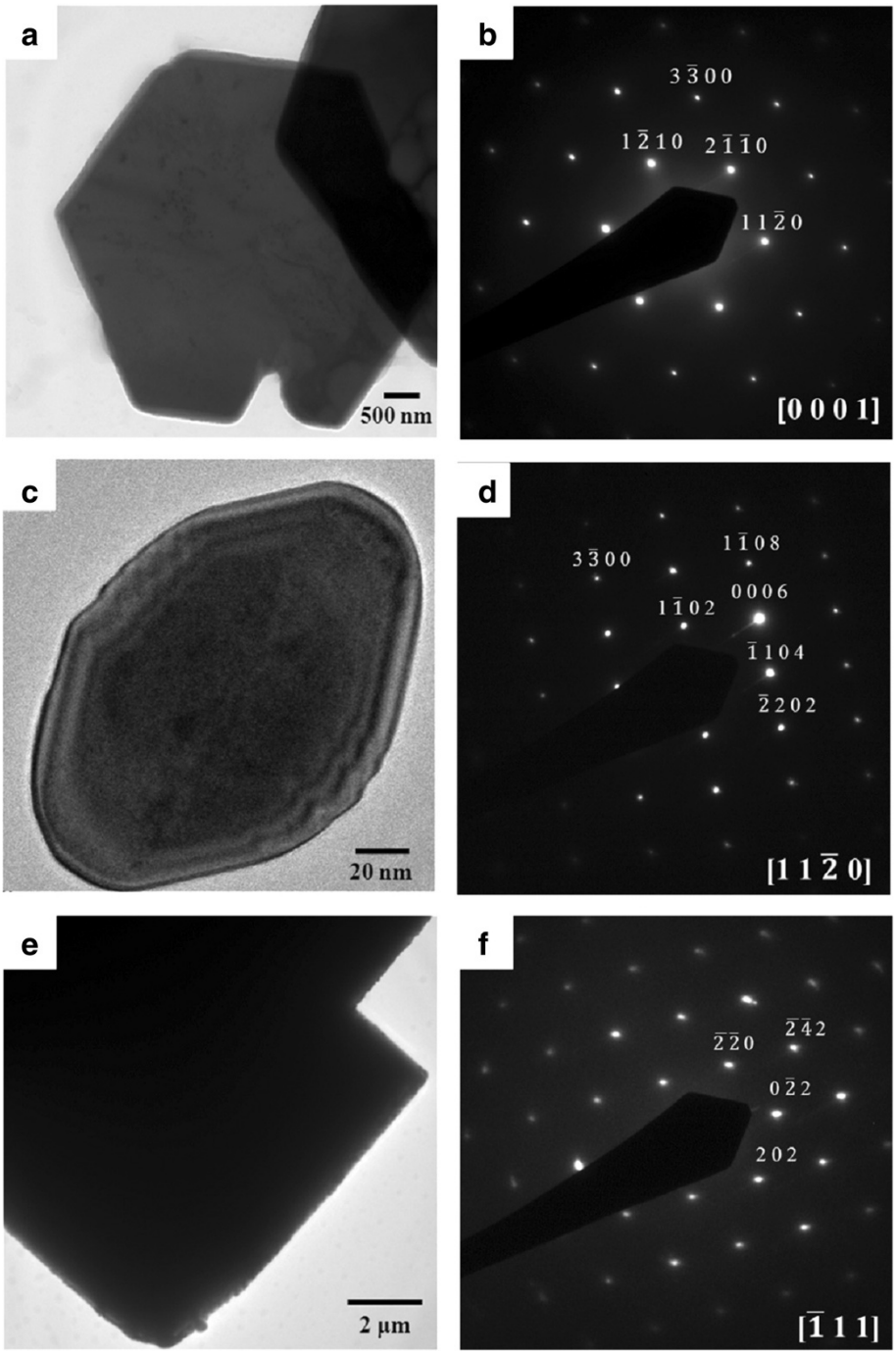

Figure 3 TEM images and SAED patterns of α-Fe_2O_3 hexagonal plates (a, b), α-Fe_2O_3 hexagonal bipyramid (c, d), and Fe_3O_4 polyhedral particles (e, f).

to be α-Fe_2O_3 when either KOH or EDA alone was added to the reaction system despite different morphologies. The diffraction peaks match the JCPDS card no. 33-0664 which is a rhombohedral structure with space group $R\bar{3}c$. The diffraction peaks obtained with the addition of both KOH and EDA into the reaction system correspond to the phase of Fe_3O_4, JCPDS card no. 19-0629, which is a face-centered cubic structure with space group $Fd\bar{3}m$. The characteristic reflections in the Fe_3O_4 phase and the γ-Fe_2O_3 phase are about the same [38]. Here diffraction of the (221), (210), and (213) planes for the γ-Fe_2O_3 phase does not exist. To further clarify the phase of polyhedral particles, the Raman spectra of α-Fe_2O_3 hexagonal plates and Fe_3O_4 polyhedral particles are shown in Figure 2. α-Fe_2O_3 here can be characterized by four strong peaks at around 225, 299, 412, and 613 cm^{-1} and two weak peaks around 247 and 497 cm^{-1}. The peaks at 538 and 668 cm^{-1} were attributed to Fe_3O_4, while the peaks at 350, 500, and 700 cm^{-1} belonging to γ-Fe_2O_3 were not observed [39,40]. The appearance of the Fe_3O_4 phase during reaction is a clear evidence that the valence change from Fe^{3+} to Fe^{2+} must occur due to the fact that Fe^{2+} ions occupy the octahedral sites of Fe_3O_4.

The α-Fe_2O_3 hexagonal plates have an average size of about 10 μm in edge length and about 500 nm in thickness. The average lateral size of the α-Fe_2O_3 particles with the shape of a hexagonal bipyramid is about 120 nm. The Fe_3O_4 polyhedral particles with mainly octahedral shape have an average lateral size in the range of 5 to 25 μm. The particles obtained from the reaction system with the addition of KOH and EDA alone have the same phase but different shapes. One would assume that the reaction system with the addition of both KOH and EDA would produce particles with maybe different shapes but still maintain the phase of α-Fe_2O_3. However, the results show that the particles that we obtained have a different phase, Fe_3O_4, and, surely, a different shape.

The transmission electron microscopy images and the corresponding selected area electron diffraction (SAED) patterns of iron oxide particles are shown in Figure 3. The diffraction patterns of the particles confirmed the results of the XRD diffractions. In Figure 3b, the zone axis of the hexagonal plate is [0001] and the six directions normal to the edge are $<2\bar{1}\bar{1}0>$ and its other five equivalent directions. In Figure 3d, the hexagonal bipyramid shows that the pyramid is pointed in the direction of <0001>. According to the literatures, the bipyramidal structure was enclosed by $\{10\bar{1}1\}$ crystal planes [41]. In Figure 3f, the Fe_3O_4 polyhedral particles which are composed of the pure magnetite phase and the diffraction spots are identified to be (202), $(0\bar{2}2)$, and $(\bar{2}\bar{2}0)$ planes and their equivalent planes under an incident electron beam along $[\bar{1}11]$.

To further understand the formation process of Fe_3O_4, the reaction systems with the addition of both KOH and EDA were hydrothermally synthesized at 200°C for different reaction times, as shown in Figure 4. Figure 4a

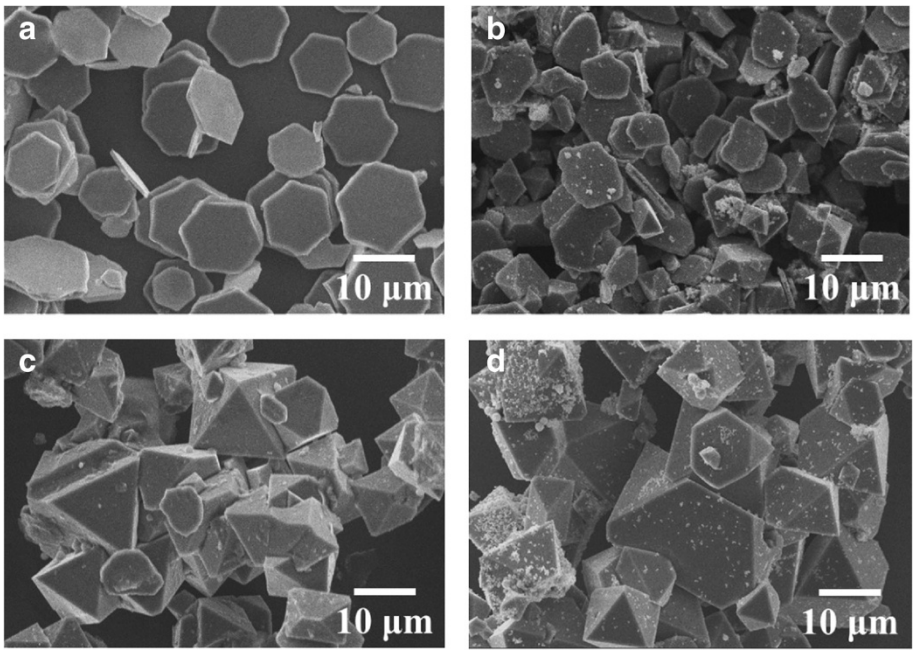

Figure 4 Mixture of α-Fe_2O_3 and Fe_3O_4 particles precipitated in the hydrothermal system at 200 °C at different times. (a) 2 h, **(b)** 5 h, **(c)** 7 h, and **(d)** 9 h.

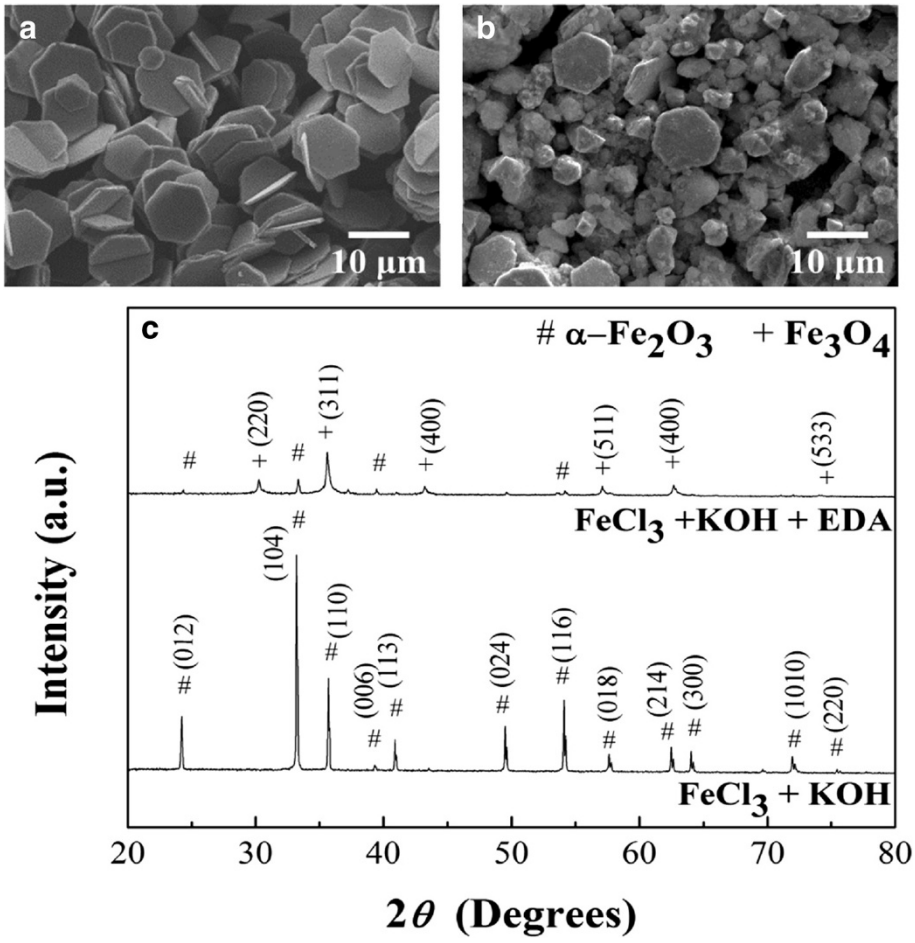

Figure 5 SEM images and corresponding XRD patterns of iron oxide particles. SEM images of iron oxide particles formed with **(a)** $FeCl_3$ + KOH and **(b)** $FeCl_3$ + KOH + EDA. **(c)** The corresponding XRD patterns of iron oxide obtained for the cases of **(a)** and **(b)**.

shows that, after 2 h of growth, the main phase of the particles is α-Fe_2O_3 hexagonal plates. The edge of the hexagonal plate is not as straight as that obtained for the reaction system with KOH only. As the reaction time increased to 5 h, as shown in Figure 4b, small octahedron particles were observed and the original hexagonal plate started to dissolve and no longer maintained the hexagonal shape. As the reaction time continued to increase to 7 h, more polyhedron particles were observed with larger sizes and only a small amount of plate-like particles still existed, as shown in Figure 4c. At the reaction time of 9 h, the observed particles are mainly polyhedron ones, as shown in Figure 4d. The first observation in this sequence of experiment is that KOH can rapidly transform iron hydroxides to hematite. The second observed phenomenon is that the α-Fe_2O_3 hexagonal plates were dissolved to become irregular plates during the transformation process.

The result implied that phase transformation evolved in four steps: (1) the reaction systems rapidly transformed Fe

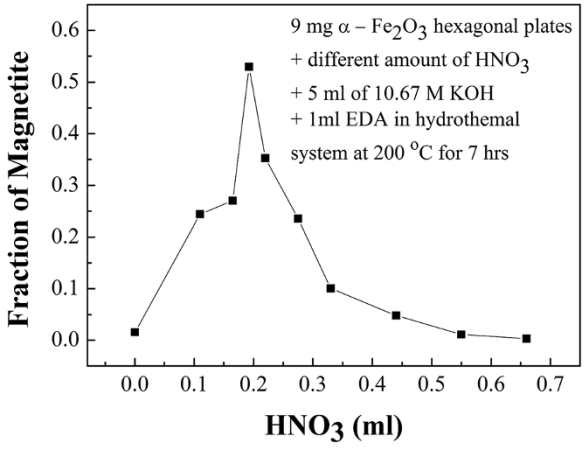

Figure 6 The fraction of magnetite transformed with different amounts of HNO_3. HNO_3 was added to 9 mg of pre-synthesized α-Fe_2O_3, 5 ml of 10.67 M KOH, and 1 ml of EDA under hydrothermal process at 200°C for 7 h.

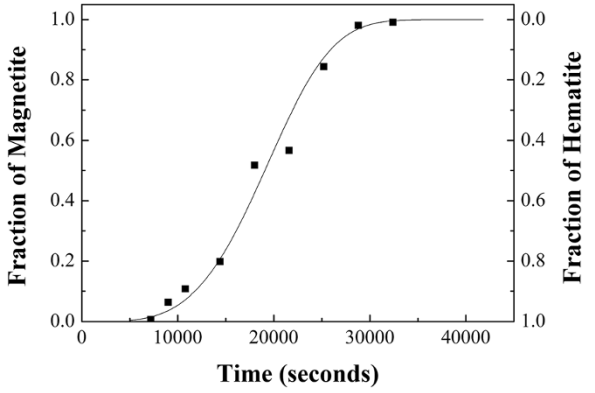

Figure 7 The fraction of magnetite transformed as a function of reaction time for $Fe(NO_3)_3$, KOH, and EDA. Under hydrothermal reaction at 200°C.

$(OH)_3$ or FeOOH to α-Fe_2O_3 hexagonal plates under the hydrothermal conditions, (2) the α-Fe_2O_3 hexagonal plates dissolved gradually, (3) the reduction process causes valence transition of Fe^{3+} to Fe^{2+}, and (4) the Fe_3O_4 particles started to nucleate and then finally grew to form polyhedral particles.

To further understand the role of NO_3^- ions on the phase transition process, the precursor of $FeNO_3$ was substituted by $FeCl_3$ with the same hydrothermal conditions. Two cases were investigated, one with the addition of KOH only and the other with the addition of both KOH and EDA under the same hydrothermal condition of 200°C for 9 h. Figure 5a shows that the α-Fe_2O_3 hexagonal plates were obtained when the reaction system consists of $FeCl_3$ and KOH, while the phase transformation from α-Fe_2O_3 hexagonal plates to Fe_3O_4 polyhedral particles still occurred when the reaction system consists of $FeCl_3$, KOH, and EDA, as shown in Figure 5b. The shape of the polyhedral particles is more irregular in this case. The XRD patterns, shown in Figure 4c, confirmed the related phases. Notice that the α-Fe_2O_3 plates were not completely reduced to Fe_3O_4 particles. Thus, NO_3^- ions are not directly involved in the reduction process of Fe^{3+} to Fe^{2+}. However, the transformation process is faster with the presence of NO_3^- ions in the reaction system than that of Cl^- ions.

We further explore the role that NO_3^- ions play on the phase transition. The pre-synthesized α-Fe_2O_3 hexagonal plates of 9 mg were added to the same KOH and EDA medium as above but with different amounts of HNO_3 and heated to 200°C for 7 h. As shown in Figure 6, the results show that the phase transition rates were slow when the solution contained large and small amounts of HNO_3; the optimal amount of HNO_3 for phase transition is 0.19 ml. The slow phase transition rate observed for small amount of HNO_3 may be attributed to the limiting dissolution of α-Fe_2O_3 which produced Fe^{3+} ion in the solution for further reduction to Fe^{2+}. Thus, the rate of phase transformation is slow. At large amount of HNO_3,

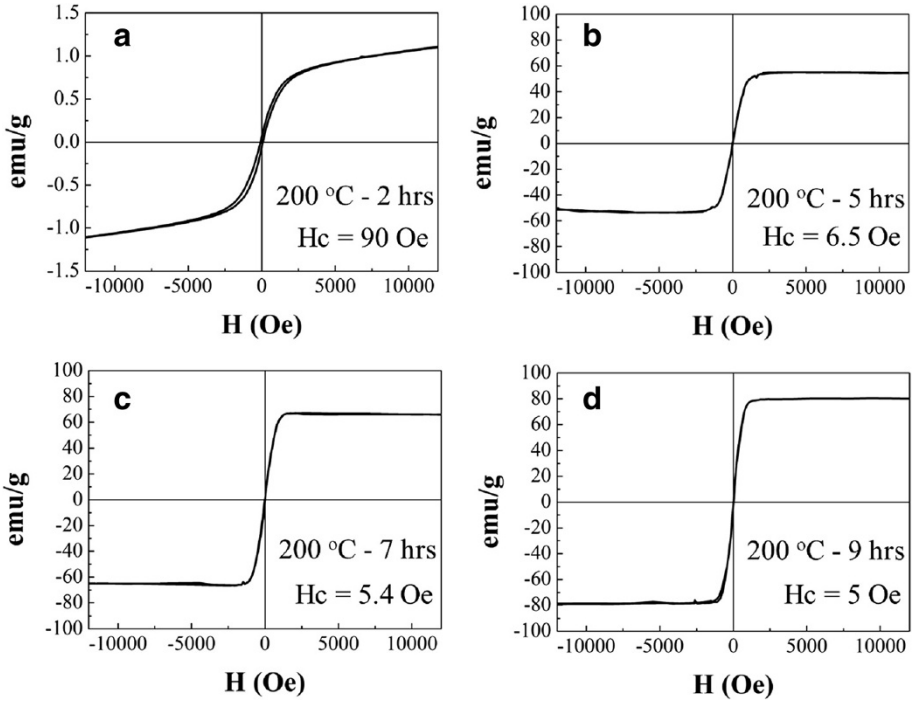

Figure 8 Magnetic properties of mixed α-Fe_2O_3 and Fe_3O_4 particles prepared by hydrothermally induced phase transformation at 200°C. (a) 2 h, **(b)** 5 h, **(c)** 7 h, and **(d)** 9 h.

the NO_3^- ions can be the oxidant in the reaction [29] and the pH value of the reaction system is changed toward a less basic solution. Hence, the reduction process can be again suppressed. Thus, there is a proper amount of HNO_3 that induces the maximum rate for phase transformation.

A similar *in situ* reduction capability of EDA in neutral and basic solutions for the reduction of uranium from U^{6+} to U^{4+} has been reported by Jouffret et al. [42]. In our study, the phase transition process should be similar. The EDA maintains stable and chelates with Fe^{3+} ions that were released by α-Fe_2O_3 hexagonal plates upon dissolving, and the reduction of Fe^{3+} ions to Fe^{2+} ions occurred.

Figure 7 shows the curve of transformed fraction of magnetite (α) as a function of reaction time. The fraction of α-Fe_2O_3 and Fe_3O_4 was determined by XRD measurement in conjunction with the Rietveld method. By using the Avrami equation, $\alpha = 1 - \exp(-kt^n)$, where k is the reaction constant, t is the reaction time, and n is the exponent of reaction, we can fit, relatively well, the experiment data of the magnetite fraction obtained by hydrothermal treatment at 200°C for different times. The value of n is about 4 obtained in this case. From this curve, we can further investigate the kinetic behavior of phase transformation in the reaction condition in the future.

The magnetic properties of iron oxide particles followed the phase transition process from α-Fe_2O_3 hexagonal plates to Fe_3O_4 polyhedral particles, as shown in Figure 8. After a short reaction time of 2 h, the α-Fe_2O_3 hexagonal plates show weak ferromagnetic behaviors with a coercive force of 90 Oe at room temperature and the saturation magnetization is yet to reach the maximum in the range of the applied magnetic field, as shown in Figure 7a. Prolonging the reaction time to 5 ~ 7 h, the fraction of Fe_3O_4 polyhedral particles as well as the particle size of Fe_3O_4 increases gradually. As shown in Figure 7b,c, the values of saturation magnetization increase to 55 and 66 emu/g and the coercive forces decrease to 6.5 and 5.4 Oe for the reaction time of 5 and 7 h, respectively. Finally, the phase transition was completed at the reaction time of 9 h. The Fe_3O_4 polyhedral particles show strong ferromagnetic behaviors with the highest saturation magnetization of 80 emu/g and the lowest coercive force of 5 Oe, as shown in Figure 7d. The magnetic properties of α-Fe_2O_3 hexagonal plates and Fe_3O_4 polyhedral particles are similar to the previous reports [27,43].

Conclusions

α-Fe_2O_3 nano/microhexagonal plates can be successfully reduced to octahedral Fe_3O_4 particles with EDA in an alkaline solution under a low-temperature hydrothermal process. In general, the transformation consists of four stages: (1) the formation of α-Fe_2O_3 hexagonal plates triggered by KOH, (2) the dissolution of the α-Fe_2O_3 hexagonal plates, (3) the reduction of Fe^{3+} to Fe^{2+}, and (4) the nucleation and growth of new Fe_3O_4 polyhedral particles. The Avrami equation can be used to describe the transformation kinetics. As the phase transformation proceeded, the magnetic properties of the sample gradually transformed from weak ferromagnetic behaviors to strong ferromagnetic behaviors.

Competing interests

The authors declare that they have no competing interests.

Authors' contributions

JFL wrote the manuscript and performed all the experiments and the data analysis. CJT provided the information and organized the final version of the paper. Both authors read and approved the final manuscript.

Authors' information

JFL is a Ph.D. student at National Tsing Hua University. CJT holds a professor position at National Tsing Hua University.

Acknowledgements

The authors acknowledge the support from the National Science Council through grant no. 101-2221-E-007-061-MY2.

Received: 7 March 2014 Accepted: 13 April 2014
Published: 13 May 2014

References

1. Wang Y, Cao J, Wang S, Guo X, Zhang J, Xia H, Zhang S, Wu S: **Facile synthesis of porous α-Fe_2O_3 nanorods and their application in ethanol sensors.** *J Phys Chem C* 2008, **112:**17804–17808.
2. Souza FL, Lopes KP, Longo E, Leite ER: **The influence of the film thickness of nanostructured α-Fe_2O_3 on water photooxidation.** *Phys Chem Chem Phys* 2009, **11:**1215–1219.
3. Wu PC, Wang WS, Huang YT, Sheu HS, Lo YW, Tsai TL, Shieh DB, Yeh CS: **Porous iron oxide based nanorods developed as delivery nanocapsules.** *Chem Eur J* 2007, **13:**3878–3885.
4. Zou Y, Kan J, Wang Y: **Fe_2O_3-graphene rice-on-sheet nanocomposite for high and fast lithium ion storage.** *J Phys Chem C* 2011, **115:**20747–20753.
5. Dong FZ, Ling DS, Chun JJ, Zheng GY, Li PY, Chun HY: **Hierarchical assembly of SnO_2 nanorod arrays on α-Fe_2O_3 nanotubes: a case of interfacial lattice compatibility.** *J Am Chem Soc* 2005, **127:**13492–13493.
6. Reda SM: **Synthesis of ZnO and Fe_2O_3 nanoparticles by sol–gel method and their application in dye-sensitized solar cells.** *Mater Sci Semicond Process* 2010, **13:**417–425.
7. Zhang S, Chen X, Gu C, Zhang Y, Xu J, Bian Z, Yang D, Gu N: **The effect of iron oxide magnetic nanoparticles on smooth muscle cells.** *Nanoscale Res Lett* 2009, **4:**70–77.
8. Kallumadil M, Tada M, Nakagawa T, Abe M, Southern P, Pankhurst QA: **Suitability of commercial colloids for magnetic hyperthermia.** *J Magn Magn Mater* 2009, **321:**1509–1513.
9. Thapa D, Palkar VR, Kurup MB, Malik SK: **Properties of magnetite nanoparticles synthesized through a novel chemical route.** *Mater Lett* 2004, **58:**2692–2694.
10. Zhang D, Liu Z, Han S, Li C, Lei B, Stewart MP, Tour JM, Zhou C: **Magnetite (Fe_3O_4) core-shell nanowires: synthesis and magnetoresistance.** *Nano Lett* 2004, **4:**2151–2155.
11. Yu MK, Jeong YY, Park J, Park S, Kim JW, Min JJ, Kim K, Jon S: **Drug-loaded superparamagnetic iron oxide nanoparticles for combined cancer imaging and therapy in vivo.** *Angew Chem Int Ed* 2008, **47:**5362–5365.
12. Zeng H, Li J, Liu JP, Wang ZL, Sun S: **Exchange-coupled nanocomposite magnets by nanoparticle self-assembly.** *Nature* 2002, **420:**395–398.
13. Kay A, Cesar I, Gratzel M: **New benchmark for water photooxidation by nanostructured α-Fe_2O_3 films.** *J Am Chem Soc* 2006, **128:**15714–15721.

14. Karunakaran C, Anilkumarl P: **Semiconductor-catalyzed solar photooxidation of iodide ion.** *J Mol Catal A Chem* 2007, **265:**153–158.
15. Geng BY, Ma JZ, You JH: **Controllable synthesis of single-crystalline Fe_3O_4 polyhedra possessing the active basal facets.** *Cryst Growth Des* 2008, **8:**1443–1447.
16. Zhang GY, Xu YY, Gao DZ, Sun YQ: **α-Fe_2O_3 nanoplates: PEG-600 assisted hydrothermal synthesis and formation mechanism.** *J Alloys Compd* 2011, **509:**885–890.
17. Yin W, Chen X, Cao M, Hu C, Wei B: **α-Fe_2O_3 nanocrystals: controllable SSA-assisted hydrothermal synthesis, growth mechanism, and magnetic properties.** *J Phys Chem C* 2009, **113:**15897–15903.
18. Liu L, Kou HZ, Mo W, Liu H, Wang Y: **Surfactant-assisted synthesis of alpha-Fe_2O_3 nanotubes and nanorods with shape-dependent magnetic properties.** *J Phys Chem B* 2006, **110:**15218–15223.
19. Nasibulin AG, Rackauskas S, Jiang H, Tian Y, Mudimela PR, Shandakov SD, Nasibulina LI, Sainio J, Kauppinen EI: **Simple and rapid synthesis of α-Fe_2O_3 nanowires under ambient conditions.** *Nano Res* 2009, **2:**373–379.
20. Ramesh R, Ashok K, Bhalero GM, Ponnusamy S, Muthamizhchelvan C: **Synthesis and properties of α-Fe_2O_3 nanorods.** *Cryst Res Technol* 2010, **45:**965–968.
21. Zhang Z, Hossain MF, Takahashi T: **Self-assembled hematite (α-Fe_2O_3) nanotube arrays for photoelectrocatalytic degradation of azo dye under simulated solar light irradiation.** *Appl Catal B Environ* 2010, **95:**423–429.
22. Hu X, Yu JC, Gong J, Li Q, Li G: **α-Fe_2O_3 nanorings prepared by a microwave-assisted hydrothermal process and their sensing properties.** *Adv Mater* 2007, **19:**2324–2329.
23. Chen D, Gao L: **A facile route for high-throughput formation of single-crystal α-Fe_2O_3 nanodisks in aqueous solutions of Tween 80 and triblock copolymer.** *Chem Phys Lett* 2004, **395:**316–320.
24. Qin W, Yang C, Yi R, Gao G: **Hydrothermal synthesis and characterization of single-crystalline α-Fe_2O_3 nanocubes.** *J Nanomater* 2011, **2011** (159259):5.
25. Liu G, Deng Q, Wang H, Ng DHL, Kong M, Cai W, Wang G: **Micro/nanostructured α-Fe_2O_3 spheres: synthesis, characterization, and structurally enhanced visible-light photocatalytic activity.** *J Mater Chem* 2012, **22:**9704–9713.
26. Nishino D, Nakafuji A, Yang JM, Shindo D: **Precise morphology analysis on platelet-type hematite particles by transmission electron microscopy.** *ISIJ Int* 1998, **38:**1369–1374.
27. Peng D, Beysen S, Li Q, Sun Y, Yang L: **Hydrothermal synthesis of monodisperse α-Fe_2O_3 hexagonal platelets.** *Particuology* 2010, **8:**386–389.
28. Yu W, Zhang T, Zhang J, Qiao X, Yang L, Liu Y: **The synthesis of octahedral nanoparticles of magnetite.** *Mater Lett* 2006, **60:**2998–3001.
29. Li Z, Kawashita M, Araki N, Mitsumori M, Hiraoka M, Doi M: **Preparation of magnetic iron oxide nanoparticles for hyperthermia of cancer in a $FeCl_2$–$NaNO_3$–NaOH aqueous system.** *J Biomater Appl* 2011, **25:**643–661.
30. Zielinski J, Zglinickab I, Znaka L, Kaszkur Z: **Reduction of Fe_2O_3 with hydrogen.** *Appl Catal A Gen* 2010, **381:**191–196.
31. Viswanath RP, Viswanathan B, Sastri MVC: **Kinetics of reduction of Fe_2O_3 to Fe_3O_4 by the constant temperature differential thermal analysis method.** *Thermochim Acta* 1976, **16:**240–244.
32. Yanagisawa K, Yamasaki N: **Reduction of haematite to magnetite under controlled hydrothermal conditions with hydrogen gas.** *J Mater Sci* 1991, **26:**473–478.
33. Ge J, Hu Y, Biasini M, Beyermann WP, Yinty Y: **Superparamagnetic magnetite colloidal nanocrystal clusters.** *Angew Chem Int Ed* 2007, **46:**4342–4345.
34. Qu S, Yang H, Ren D, Kan S, Zou G, Li D, Li M: **Magnetite nanoparticles prepared by precipitation from partially reduced ferric chloride aqueous solutions.** *J Colloid Interface Sci* 1999, **215:**190–192.
35. Sapieszko RS, Matijewic E: **Preparation of well-defined colloidal particles by thermal decomposition of metal chelates.** *J Colloid Interface Sci* 1980, **74:**405–422.
36. Mitra S, Das S, Mandal K, Chaudhuri S: **Synthesis of a α-Fe_2O_3 nanocrystal in its different morphological attributes: growth mechanism, optical and magnetic properties.** *Nanotechnology* 2007, **18**(275608):9.
37. Wan J, Chen X, Wang Z, Yang X, Qian Y: **A soft-template-assisted hydrothermal approach to single-crystal Fe_3O_4 nanorods.** *J Cryst Growth* 2005, **276:**571–576.
38. Khollam YB, Dhage SR, Potdar HS, Deshpande SB, Bakare PP, Kulkarni SD, Date SK: **Microwave hydrothermal preparation of submicron-sized spherical magnetite (Fe_3O_4) powders.** *Mater Lett* 2002, **56:**571–577.
39. Slavov L, Abrashev MV, Merodiiska T, Gelev C, Vandenberghe RE, Markova-Deneva I, Nedkovt I: **Raman spectroscopy investigation of magnetite nanoparticles in ferrofluids.** *J Magn Magn Mater* 2010, **322:**1904–1911.
40. Song K, Lee Y, Jo MR, Nam KM, Kang YM: **Comprehensive design of carbon-encapsulated Fe_3O_4 nanocrystals and their lithium storage properties.** *Nanotechnology* 2012, **23**(505401):6.
41. Lv B, Liu Z, Tian H, Xu Y, Wu D, Sun Y: **Single-crystalline dodecahedral and octodecahedralα-Fe_2O_3 particles synthesized by a fluoride anion-assisted hydrothermal method.** *Adv Funct Mater* 2010, **20:**3987–3996.
42. Jouffret L, Rivenet M, Abraham F: **Linear alkyl diamine-uranium-phosphate systems: U(VI) to U(IV) reduction with ethylenediamine.** *Inorg Chem* 2011, **50:**4619–4626.
43. Zhang W, Gai L, Li Z, Jiang H, Ma W: **Low temperature hydrothermal synthesis of octahedral Fe_3O_4 microcrystals.** *J Phys D Appl Phys* 2008, **41:**225001–225007.

doi:10.1186/1556-276X-9-230
Cite this article as: Lu and Tsai: Hydrothermal phase transformation of hematite to magnetite. *Nanoscale Research Letters* 2014 **9**:230.